Climate Dynamics (1999) 15:875–893

E. C. Wiebe · A. J. Weaver

On the sensitivity of global warming experiments to the parametrisation of sub-grid scale ocean mixing

Received: 14 October 1998 / Accepted: 27 April 1999

Abstract An ocean general circulation model coupled to an energy-moisture balance atmosphere model is used to investigate the sensitivity of global warming experiments to the parametrisation of sub-grid scale ocean mixing. The climate sensitivity of the coupled model using three different parametrisations of sub-grid scale mixing is 3 °C for a doubling of CO_2 (6 °C for a quadrupling of CO_2). This suggests that the ocean has only a weak feedback on global mean surface air temperature although significant regional differences, notably at high latitudes, exist with different sub-grid scale parametrisations. In the experiment using the Gent and McWilliams parametrisation for mixing associated with mesoscale eddies, an enhancement of the surface response in the Southern Ocean is found. This enhancement is largely due to the existence of more realistic sea-ice in the climatological control integration and the subsequent enhanced ice-albedo feedback upon warming. In accordance with earlier analyses, the Gent and McWilliams scheme decreases the global efficiency of ocean heat uptake. During the transient phase of all experiments, the North Atlantic overturning initially weakened but ultimately recovered, surpassing its former strength. This suggests that in the region around the North Atlantic the ocean acts as a negative feedback on local warming during the transient phase but a positive feedback at equilibrium. During the transient phase of the experiments with a more sophisticated and realistic parametrisation of sub-grid scale mixing, warmed Atlantic water was found to penetrate at depth into the Arctic, consistent with recent observations in the region.

E. C. Wiebe (✉) A. J. Weaver
School of Earth and Ocean Sciences, University of Victoria,
PO Box 3055, Victoria, B.C., V8W 3P6, Canada

1 Introduction

The ocean, with its large heat capacity and ability to transport heat poleward, is commonly thought to play an integral part in regulating climate and climate change. Indeed, this is readily apparent through the comparison of the projections of climate change from atmospheric models coupled to mixed-layer ocean models (IPCC 1990) and ocean general circulation models (OGCMs, IPCC 1992, 1995). Both classes of models reveal reduced warming over the ocean relative to the land (due in part to the high heat capacity of the ocean), while significant differences exist between the two classes of models in regions such as the Atlantic Ocean where deep water formation occurs (due to changes in ocean heat transport allowable in OGCMs, see Weaver 1993 for a review). Since OGCMs are known to be sensitive to the parametrisation of sub-grid scale ocean mixing (Bryan 1987), and as there is a great deal of uncertainty in even the basic physics of such parametrisations, it is important to examine whether or not projections of future climate change are sensitive to the parametrisation of these unresolved ocean processes.

Gent and McWilliams (1990) recently introduced a new parametrisation of mesoscale eddy-induced mixing for use in coarse resolution ocean models. The idea was to improve ocean models by adding isopycnal thickness diffusion to account for the removal of potential energy from the stratification due to baroclinic instability. This new parametrisation has been shown to greatly improve the climatology of ocean models (Danabasoglu et al. 1994; Böning et al. 1995; Danabasoglu and McWilliams 1995; McDougall et al. 1996), including ventilation rates and the distribution of passive tracers such as CFCs (e.g. Robitaille and Weaver 1995; England 1995).

The result of Hirst et al. (1996), that the introduction of the Gent and McWilliams (1990) scheme into a coupled model enhanced the asymmetry of the model's

response to increasing atmospheric greenhouse gases, is in contrast with previous expectations (McDougall et al. 1996) and provides some of the impetus for our study. Here we use the recently developed energy-moisture balance model (EMBM) of Fanning and Weaver (1996) coupled to the GFDL MOM2 OGCM (Pacanowski 1995) and to a thermodynamic ice model based upon Semtner (1976) and Hibler (1979). The simplicity of the atmospheric component of the coupled model allows the coupled system to be integrated through the transient phase of an imposed radiative forcing to equilibrium without the use of explicit flux adjustments. In addition, computational efficiency allows us to conduct numerous sensitivity analyses.

The outline is as follows: in the next section we briefly describe the model and the design of the experiments, including the details of the forcing used to represent increasing concentrations of atmospheric CO_2. We then present (Sect. 3) the climatology obtained after integrating the coupled model to equilibrium under present-day forcing with various sub-grid scale mixing parametrisations. We describe the coupled model response to increasing atmospheric CO_2, beginning with the equilibrium response in Sect. 4, and then moving to the transient response in Sect. 5. We discuss our results and summarise our main findings in Sect. 6.

2 The coupled model and experimental design

The global coupled model is configurated with a meridional resolution of 1.8555° and a zonal resolution of 3.75°, extending to the pole in the Northern Hemisphere, where an artificial island was inserted due to the convergence of meridians and the potential existence of a singularity there. In the Southern Hemisphere the grid extends to 79 °S, while in the vertical there are 19 levels, varying from 50 m thickness at the first level to 600 m thickness at the deepest level (with a maximum ocean depth of 5400 m). In all cases momentum dissipation is accomplished through the use of a Laplacian operator acting in the horizontal and vertical directions, with viscosity coefficients of $A_h = 2.5 \times 10^5\ \mathrm{m^2\,s^{-1}}$ in the horizontal and $A_v = 1.0 \times 10^{-3}\ \mathrm{m^2\,s^{-1}}$ in the vertical.

The EMBM is a vertically-integrated model of the atmosphere which was designed to be extremely efficient, yet sufficiently realistic, to allow for its use in long-time-scale climate integrations. When coupled to an ocean model, the EMBM allows the realistic air/sea feedbacks at the ocean surface, without the need for explicit flux adjustments. As the EMBM contains no explicit dynamics, monthly mean values of wind stress from de Silva et al. (1994) were interpolated spatially and temporally onto the model grid and retained throughout all experiments. The solar insolation was also recalculated at each time-step based on present day orbital parameters. This, in conjunction with the monthly wind fields, allowed us to simulate the seasonal cycle. The wind stress field was also converted to a wind speed field for use in the model calculation of latent and sensible heat fluxes at the air-sea interface. In the experiments shown, a wind stress feedback parametrisation (Fanning and Weaver 1997a) was not used although all experiments were repeated with this feedback turned on, with no change in our results.

Atmospheric heat and fresh water transports in the EMBM are parametrised through Fickian diffusion and precipitation is assumed to occur in the model whenever the relative humidity reached greater than 85%. Precipitation over land is assumed to instantaneously return to the ocean via one of 21 river drainage basins (see Weaver et al. 1998). Ice-albedo feedbacks were also incorporated into the coupled model whenever sea ice was present and whenever the SAT over land was below $-10\,^{\circ}\mathrm{C}$, by locally reduced the latitudinal profile of the coalbedo by 0.1 (Graves et al. 1993). More details regarding the ocean component of the coupled model can be found in Weaver and Hughes (1996) while the EMBM and thermodynamic ice model are discussed in Fanning and Weaver (1996).

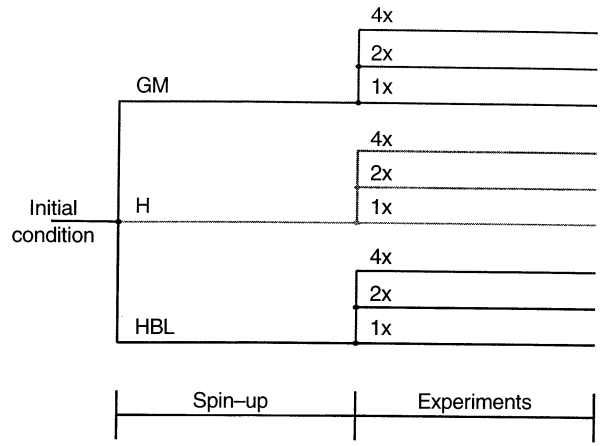

Fig. 1 Schematic diagram of the experiments conducted in this study. 1x represents the equilibrium present-day control equilibrium while 2x and 4x represent transient CO_2-increase experiments which are then integrated to equilibrium once CO_2 has doubled or quadrupled, respectively. The three sub-grid scale mixing schemes used are: horizontal with constant vertical diffusivity (*H*); horizontal with depth-varying (Bryan and Lewis 1979) vertical diffusivity (*HBL*); the Gent and McWilliams (1990) parametrisation (*GM*). The initial condition consists of a horizontally-homogeneous ocean and dry, isothermal atmosphere

Three series of experiments were conducted with each series characterised by the particular sub-grid scale diffusion parametrisation used (see Fig. 1). In the first series of experiments, denoted H, the traditional Laplacian diffusion operator was incorporated with a horizontal diffusivity of $k_h = 2.0 \times 10^3\ \mathrm{m^2\,s^{-1}}$ and a vertical diffusivity of $k_v = 1.0 \times 10^{-4}\ \mathrm{m^2\,s^{-1}}$. The second series, denoted HBL, was the same as H except that we used a vertically-varying vertical diffusivity (taken from Bryan and Lewis 1979) which corresponded to $k_v = 0.3 \times 10^{-4}\ \mathrm{m^2\,s^{-1}}$ at the surface, increasing to $k_v = 1.3 \times 10^{-4}\ \mathrm{m^2\,s^{-1}}$ at the deepest model level. In the last series, entitled GM, we replaced the horizontal/vertical mixing scheme by the Gent and McWilliams (1990) parametrisation. This involved rotating the diffusion tensor along isopycnals (using the Griffies et al. 1998 method), setting the isopycnal diffusivity to $k_i = 2.0 \times 10^3\ \mathrm{m^2\,s^{-1}}$, retaining the same vertical diffusivity as in H, and setting the horizontal diffusivity to zero. In addition, isopycnal thickness diffusion was added (with a diffusivity of $k_t = 2.0 \times 10^3\ \mathrm{m^2\,s^{-1}}$). While we initially wished to conduct a fourth series of experiments with the Gent and McWilliams (1990) parametrisation included along with the Bryan and Lewis (1979) vertically-varying vertical diffusivity, the present-day climatology corresponding with this combination of mixing schemes did not have deep water formation in the North Atlantic, making it unsuitable as a possible realisation of the present climate. Control climatologies were obtained for each H, HBL and GM by integrating the coupled model to equilibrium (for 5000 y) starting from a resting, horizontally-homogeneous ocean and dry, isothermal atmosphere.

The EMBM includes a parametrisation of the water vapour/planetary longwave feedback (Thompson and Warren 1982), although the radiative forcing associated with increasing greenhouse gases (here combined into a CO_2 equivalent) was externally imposed

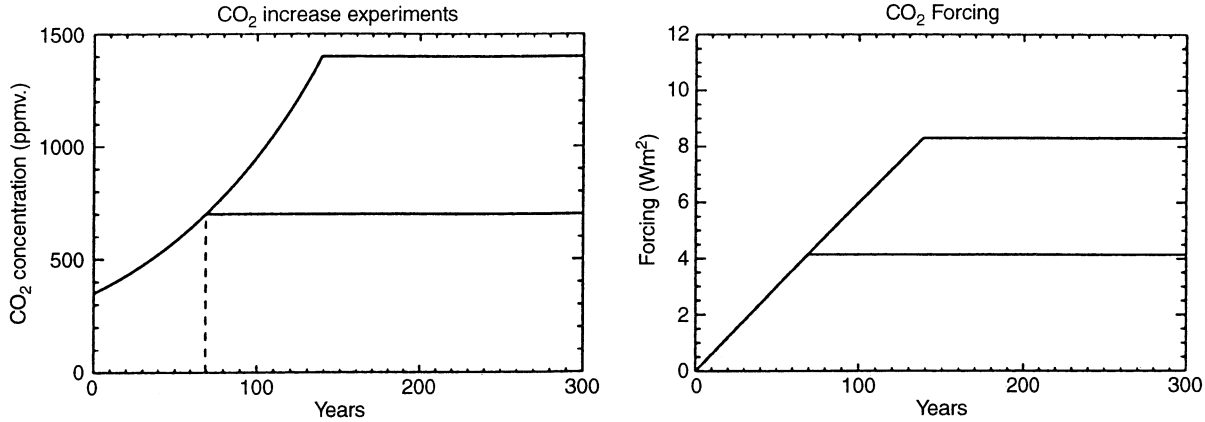

Fig. 2 CO_2 concentration (ppm) and equivalent radiative forcing (Wm^{-2}) as a function of time from the beginning of the perturbation experiments. For each of our three model configurations (H, HBL, GM) we conducted 2x and 4x experiments by allowing the atmospheric CO_2 concentration to increase until the time of doubling (2x) or quadrupling (4x), after which time the CO_2 concentration was kept constant until a new equilibrium was reached

as a reduction of the planetary long wave radiation flux (see also Fanning and Weaver 1997b). The anthropogenic forcing $\Delta F(t)$ was calculated using

$$\Delta F(t) = \Delta F_{2x} ln\left(\frac{C(t)}{C_0}\right). \quad (1)$$

In accordance with Ramanathan et al. (1987) we specify ΔF_{2x} to give a radiative forcing of 4 Wm^{-2} at the time of CO_2 doubling. In our experiments we increased the concentration of CO_2 ($C(t)$) at a rate of 1% compounded per year (following the "business-as-usual" scenario of IPCC 1990) starting from a present-day concentration of $C_0 = 350$ ppm. For each of our three model configurations (H, HBL, GM) we conducted 2x and 4x experiments by allowing the atmospheric CO_2 concentration to increase until the time of doubling (2x) or quadrupling (4x), after which time the CO_2 concentration was kept constant until a new equilibrium was reached (after a total to 3000 y of integration). The atmospheric CO_2 concentration and its associated radiative forcing throughout the transient phase of these experiments are shown in Fig. 2

3 Equilibrium present-day control climatologies

The globally-averaged annual mean SAT and sea surface temperature (SST) at the end of the spin-up to equilibrium of the H, HBL and GM control climatologies are shown in Table 1. While all three present-day realisations yield similar values, the SAT from our control climates are about 1 °C cooler than observational estimates (approximately 14 °C with the mean temperature of Northern Hemisphere winter being 12.4 °C and that of northern hemisphere summer, 15.9 °C—IPCC 1995). Nevertheless, our values are not unrealistic and are in fact about 1.5 °C warmer than the global mean screen temperature of the *standard* integration of Manabe and Stouffer (1994, see their Fig. 2).

Upon first glance, the spatial SAT distribution at the equilibrium of the three control experiments appear similar, although difference plots (Fig. 3) reveal subtle

Table 1 Globally-averaged annual mean equilibrium sea surface (SST) and surface air (SAT) temperatures at the equilibrium of the three climatological control experiments

Experiments	SST (°C)	SAT (°C)
H	15.82	12.81
HBL	15.96	12.75
GM	15.98	12.67

changes between the H, HBL and GM climatologies. The most notable differences occur in the tropics, where HBL is warmer than H and GM; in the Southern Ocean, where GM is warmer than H and HBL; at high latitudes where HBL and GM are colder than H. As the atmospheric component of our coupled model is simple, the horizontal SAT inter-model anomaly distribution represents a smoothed (through atmospheric diffusion) version of the SST intermodel anomaly fields (Fig. 4).

In the tropics, where isopycnals are approximately horizontal, the values chosen for the vertical and horizontal mixing in the H experiment are similar to those in the GM case. The HBL experiment on the other hand limits vertical mixing between the surface levels, allowing the tropical SSTs to be warmer than in the other two experiments. At high latitudes, especially in the Southern Hemisphere, the GM and HBL control models produce SSTs more similar to each other than to those of the H model. In this case this is due to the fact that the GM and HBL models constrain convection by increasing the stratification of the ocean. The suppression of unrealistic large areas of deep convection (that exist in H) causes the surface layers to become colder when exposed to cold polar air. The result is that sea ice is also more extensive in HBL and GM, especially in the Southern Hemisphere (Table 2; bold line

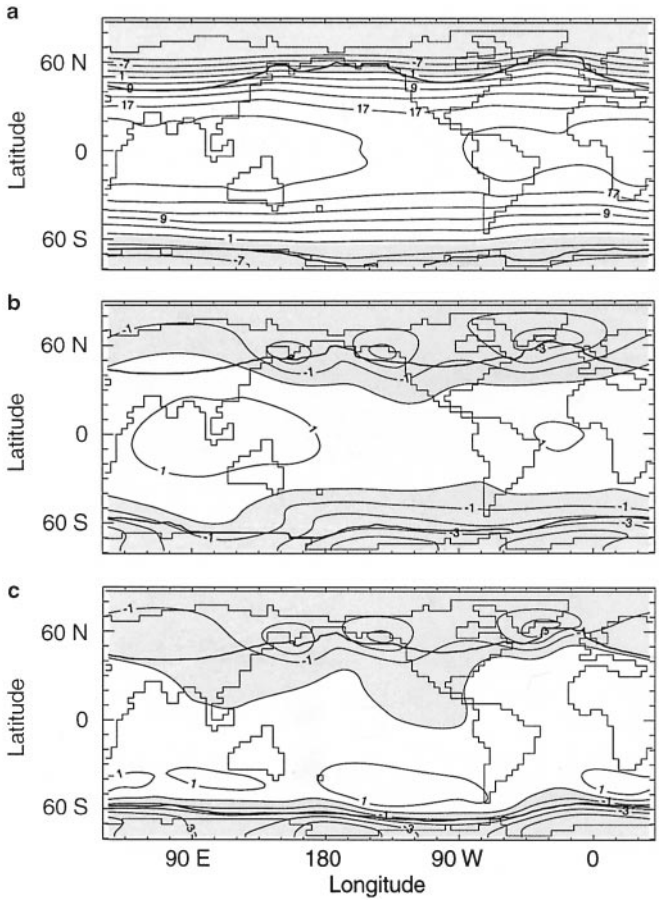

Fig. 3 **a** Annual mean surface air temperature (°C) for the present-day climatology of the H model. **b** As in **a** but for differences between HBL and H (HBL − H). **c** As in **b** except for the GM model. The contour interval is 4 °C in **a** and 1 °C in **b** and **c**. *Shaded areas* in **a** indicate regions colder than 0 °C, while in **b** and **c** they show regions colder than in the H model. The *thick solid line* gives the annual mean sea ice extent (> 0%) over the ocean and the latitude of the −10 °C contour over land in each of the respective climatologies

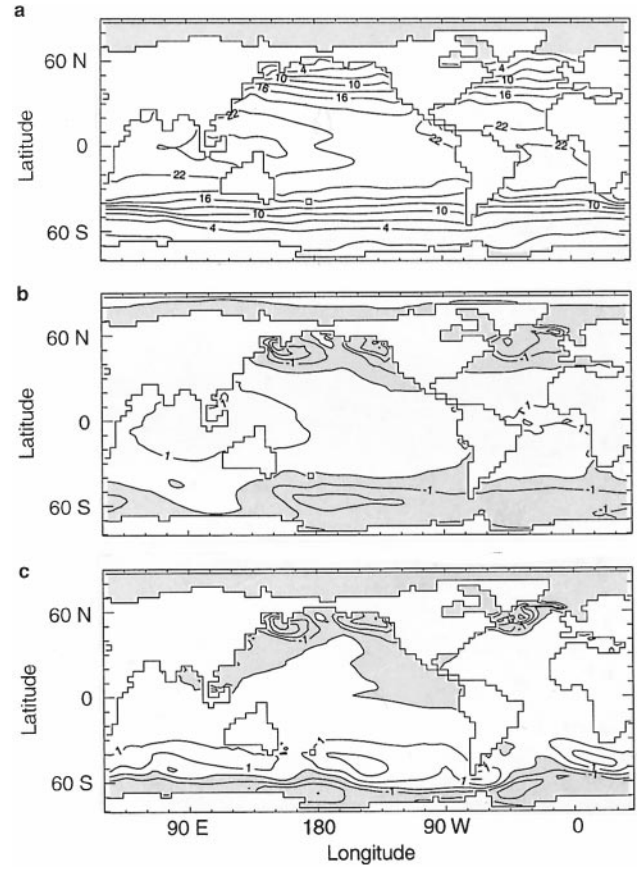

Fig. 4a–c As in Fig. 3 but for sea surface temperature. The contour interval in **a** is 3 °C, while in **b** and **c** it is 1 °C. *Shaded areas* in **a** are colder than 0 °C, while in **b** and **c** they represent regions colder than the H model

Table 2 Global and hemispheric ice covered area for all experiments. SH and NH are the Southern and Northern hemispheres, respectively

Experiment	Total ($\times 10^6$ km^2)	SH ($\times 10^6$ km^2)	NH ($\times 10^6$ km^2)
H	11.9	0.7	11.2
H2x	8.5	0.0	8.5
H4x	6.5	0.0	6.5
HBL	19.7	6.1	13.6
HBL2x	11.0	0.6	10.4
HBL4x	8.3	0.0	8.3
GM	20.8	7.7	13.2
GM2x	12.0	2.1	9.9
GM4x	6.5	0.3	6.2

in Fig. 3), where the subsequent ice-albedo feedback further cools the region. The ice cover is too extensive in the North Atlantic in all models due to the coarse resolution of the model which results in a relatively weak Gulf Stream and correspondingly poor penetration of warm near surface water in the northernmost North Atlantic.

In the Southern Ocean, the eddy-induced bolus transport associated with the Gent and McWilliams (1990) scheme largely cancels out the vertical overturning cell (known as the Deacon Cell) associated with the northward Ekman transport of cold surface waters and subsequent return flow at depth (Danabasoglu et al. 1994). In addition, the alignment of diffusion along isopycnals substantially reduces unrealistic diffusive southward surface heat transport (Fig. 5), which would otherwise cause spurious deep overturning and mixed layers in the Southern Ocean. On the northern side of the Antarctic Circumpolar Current (ACC) the first process dominates, so that in the GM case large areas of the Southern Ocean are substantially warmer and more stratified than in both H and HBL. On the southern side of the ACC the second process dominates and spurious deep convection is suppressed.

It is well known that the strength of the overturning is sensitive to the value of the vertical diffusivity (Bryan

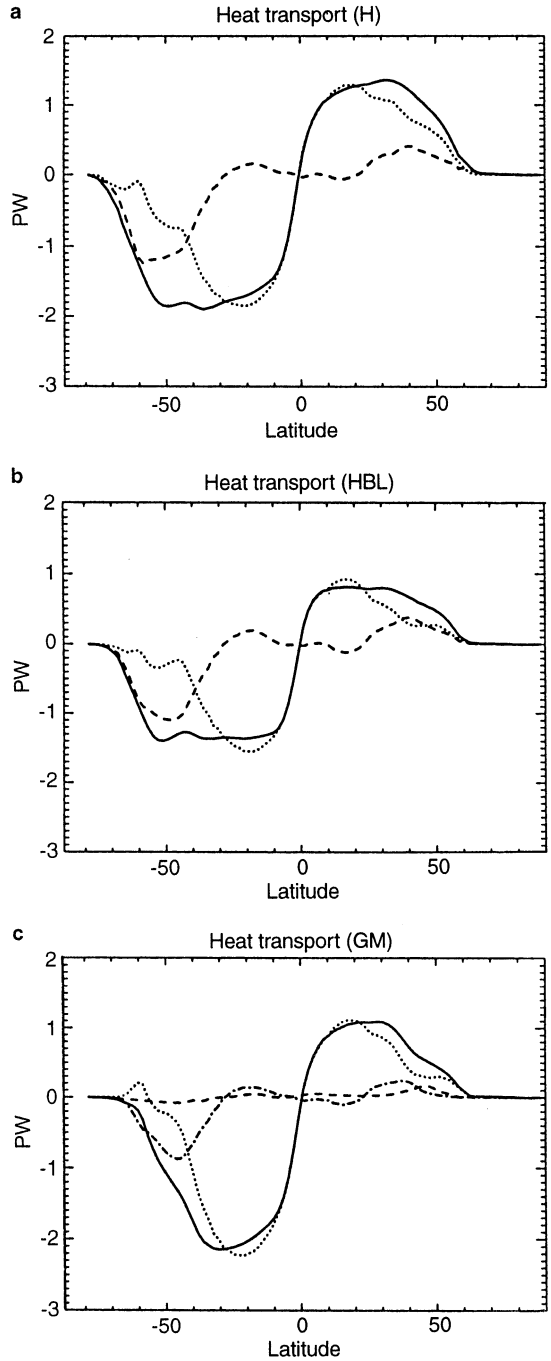

Fig. 5 a Annual mean global oceanic heat transport (PW) for the present-day equilibrium climatology of the H model. *Positive values* indicate northward heat transport. The *solid line* is the total heat transport, the *dotted line* is the component due to advection, while the *dashed line* indicates the component due to diffusion. **b** As in **a** but for the HBL model. **c** As in **a** but for the GM model. The *dash-dotted line* in **c** shows the eddy-induced bolus heat transport

1987). As such, it is not surprising to see that the HBL model has about 13 Sv of deep water formation in the North Atlantic relative to 24 Sv in H (Fig. 6a, d). This follows since in the thermocline $k_v \sim 0.3 \times 10^{-4}\,\mathrm{m^2\,s^{-1}}$ in HBL relative to $k_v = 1.0 \times 10^{-4}\,\mathrm{m^2\,s^{-1}}$ in H. As a result in the Northern Hemisphere, the poleward heat transport in HBL is the weakest (Table 3; Fig. 5) and the North Atlantic the coolest (Fig. 3) of all. The North Atlantic mass transport in GM is also around 13 Sv (similar to HBL) although when one includes the eddy-induced bolus transport the net tracer transport increases to about 15 Sv (Fig. 6g). This reduced overturning relative to H also explains the cooler North Atlantic (Fig. 4c) and reduced poleward heat transport (Table 3) in GM. Deep water formation in the North Pacific is absent in HBL and GM although there is too much production of intermediate water in the North Pacific in the H model (not shown). There is more trapping of fresh water in the upper layers of the North Pacific in the GM and HBL models which is responsible for reducing convection and thus overturning there. The deep AABW input into the North Atlantic is about 4 Sv in all the experiments.

Table 3 Maximum oceanic heat transports (PW; $1\mathrm{PW} \equiv 10^{15}\mathrm{W}$) at the equilibrium of the three control models as well as from several other coupled models and a range of observations (Russell et al. 1995). Acronyms are defined on the caption to Table 4 with GISS – Goddard Institute for Space Studies, USA

Experimental/Group	Maximum Heat Transport (PW)
H	1.4
HBL	0.8
GM	1.1
GFDL	1.5
GISS	1.4
MPI	1.3
UKMO	1.2
Observations	1.6–2.8

Due to the constraint imposed by the incoming solar radiation, it is not surprising that the planetary heat transport compares well with observations (Hartman 1994) in all our models (not shown). Nevertheless, as illustrated in Table 3 and Fig. 5 there is a tendency for our ocean to transport too little heat with the atmosphere picking up the difference. This problem is not confined to the present model but is in fact characteristic of most coarse-resolution ocean models (Table 3). Indeed, Fanning and Weaver (1997c) showed that increased resolution in the oceanic component of this coupled model results in improved oceanic heat transports primarily through better representation of western boundary currents.

The equilibrium control climates from the three models (H, HBL and GM) are integrated for a further 3000 y, in parallel with the CO_2-increase experiments (Fig. 1). The control climates, which remain stable during that integration, are used as a reference for the CO_2-increase experiments, discussed in the next two sections. We begin by examining the equilibrium response to CO_2 doubling and quadrupling before moving onto the transient response. Throughout our

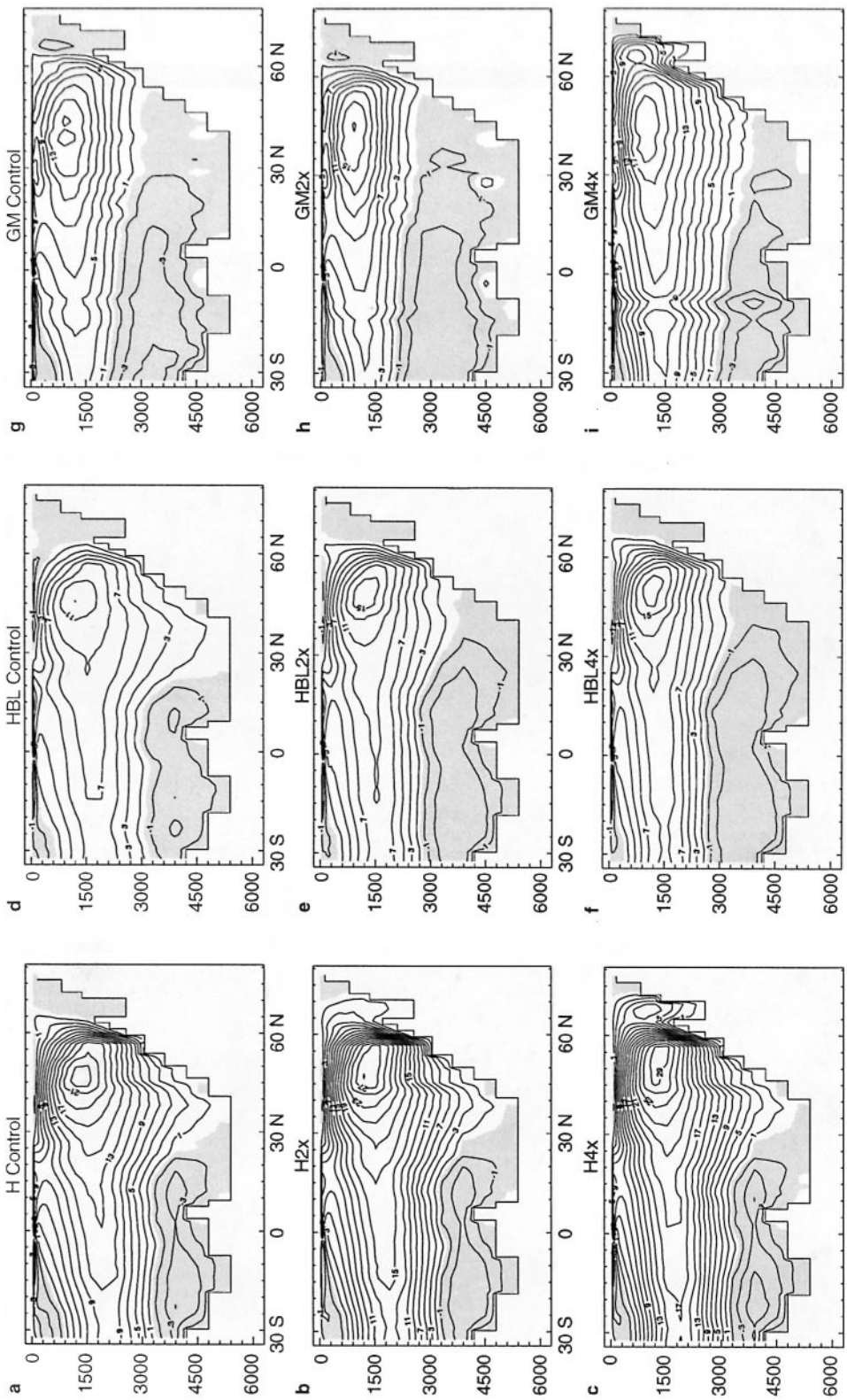

Fig. 6a–i Annual mean meridional overturning stream function (Sv; 1 Sv $\equiv 10^6$ m^3 s^{-1}) in the Atlantic Ocean for the equilibrium climatology of: **a** H; H2x; **c** H4x; **d** HBL; **e** HBL2x; **f** HBL4x; **g** GM; **h** GM2x; **i** GM4x. The contour interval is 2 Sv with *shaded areas* indicating counter-clockwise circulation. In **g–i** the stream function using the sum of both the mean and eddy-induced bolus transports is shown

Table 4 Globally-averaged annual mean equilibrium sea surface (SST) and surface air (SAT) temperature responses for the $2\times$ and $4\times CO_2$ experiments. Results from other groups (taken from IPCC 1995) are also shown at the right for comparison. All values are for $2\times$ CO_2 experiments where CO_2 was increased by 1% per year. BMRC, Bureau of Meteorology Research Centre, Australia; CCC, Canadian Centre for Climate Modelling and Analysis, Canada; CSIRO, Commonwealth Scientific and Industrial Research Organisation, Australia; GFDL, Geophysical Fluid Dynamics Laboratory, USA; MPI, Max Planck Institute for Meteorology, Germany; NCAR, National Center for Atmospheric Research, USA; UKMO, United Kingdom Meteorological Office, United Kingdom

Experiment	Δ SST (°C)	Δ SAT (°C)	Δ SAT (2x) (°C)	Group
H2x	2.26	2.89	2.1	BMRC
HBL2x	2.29	3.00	3.5	CCC
GM2x	2.28	3.01	4.3	CSIRO
H4x	4.63	5.81	3.7	GFDL
HBL4x	4.71	6.01	2.6	MPI
GM4x	4.52	6.00	4.6	NCAR
			2.7	UKMO

discussion we will focus on the effects arising from the different parametrisations of sub-grid scale mixing.

4 The equilibrium $2\times$ and $4\times CO_2$ climate response

The globally-averaged SAT and SST change (Table 4) at the equilibrium of the six (Fig. 1) CO_2-increase experiments is similar for all three mixing schemes, with a doubling of CO_2 leading to about 3.0 °C SAT (2.3 °C SST) warming and increasing linearly with the quadrupling of CO_2 to about a 6.0 °C (4.6 °C SST) warming. These numbers fall within the range of IPCC (1995) tabulated results (see Table 4), representing a weak to moderate climate sensitivity of our coupled model. The similarity of the response between the three classes of models (H, HBL, GM) suggests that on the *global average*, there is little net ocean feedback on the equilibrium SAT and SST. This result is consistent with the analysis of Weaver et al. (1998) where they concluded that ocean feedbacks in their coupled model did not contribute to the globally-averaged warming since the last glacial maximum.

While the globally-averaged SAT and SST may be similar between the H, HBL and GM models, there are substantial spatial differences between the equilibrium responses (e.g. Fig. 7 for $2\times CO_2$ and Fig. 8 for $4\times CO_2$). The greatest warming in the H2x model (Fig. 7a) took place over the high latitude North Atlantic, where the SAT increased by a maximum of 7 °C in the annual average. This is a direct result of two processes. The first involves a positive-albedo feedback, whereby the ice edge in the H model was forced back by the warming atmosphere and ocean, causing a reduction in albedo and thereby locally enhancing the warming. The zonally-averaged responses shown in Fig. 9 clearly illustrate the differences in the high-latitude responses of the three models. The second process involves a positive ocean feedback (discussed in more detail in the next section), whereby increased equilibrium North Atlantic overturning (Fig. 6b) lead to increased northward heat transport (Fig. 10a), thereby warming the region there (and contributing to enhanced ice melt and subsequent ice-albedo feedback).

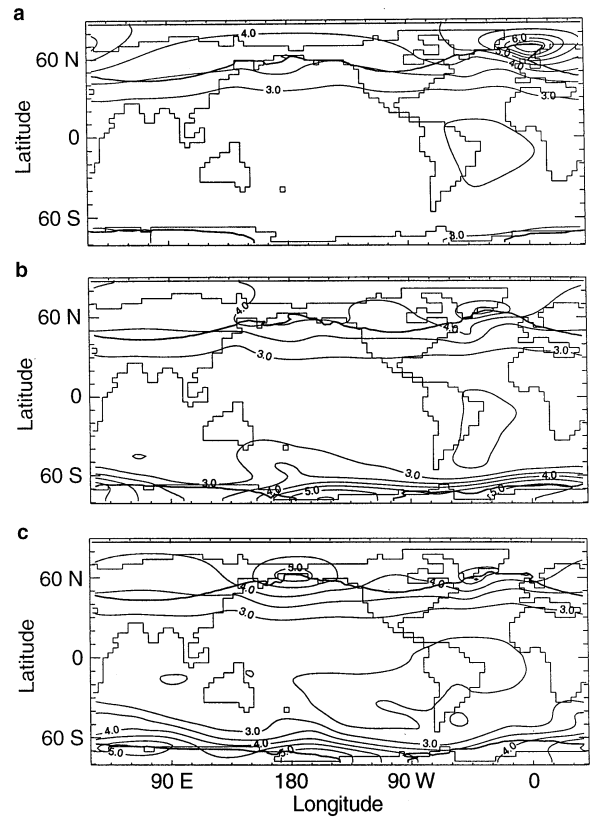

Fig. 7a–c Annual mean surface air temperature (°C) equilibrium $2\times CO_2$ response for the **a** H2x model; **b** HBL2x model; **c** GM2x model (the contour interval is 0.5 °C). The response was calculated as the difference between the 2x experiment and its respective control. The *thick solid line* gives the annual mean sea ice extent (> 0%) over the ocean and the latitude of the −10 °C contour over land

There is almost uniform warming in the Pacific, Indian and Southern Ocean of the H2x model, in contrast with the patterns of warming in the GM2x (Fig. 7b) and HBL2x models (Fig. 7c). In the latter models the southern high latitudes experience enhanced warming relative to lower latitudes. While the $2\times CO_2$ equilibrium SAT response in the H2x case has a pronounced interhemispheric asymmetry compared to the HBL2x and GM2x cases, this is not primarily due to differences in the Southern Ocean heat uptake but rather to differences in the ice-albedo feedback. The HBL and GM climatologies both have far more extensive ice cover in the Southern Ocean (Fig. 3; Table 2), resulting in a stronger ice-albedo feedback

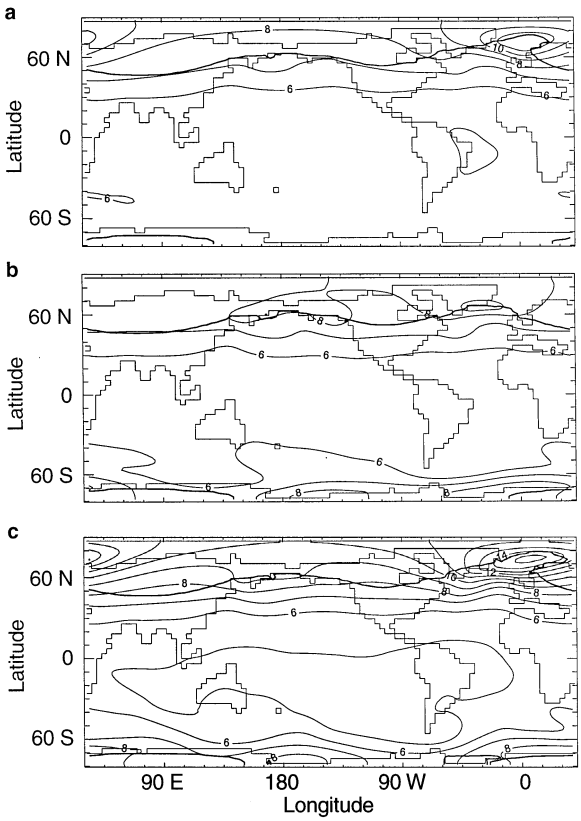

Fig. 8a–c As in Fig. 7 but for the equilibrium $4 \times CO_2$ response (the contour interval is 1.0 °C)

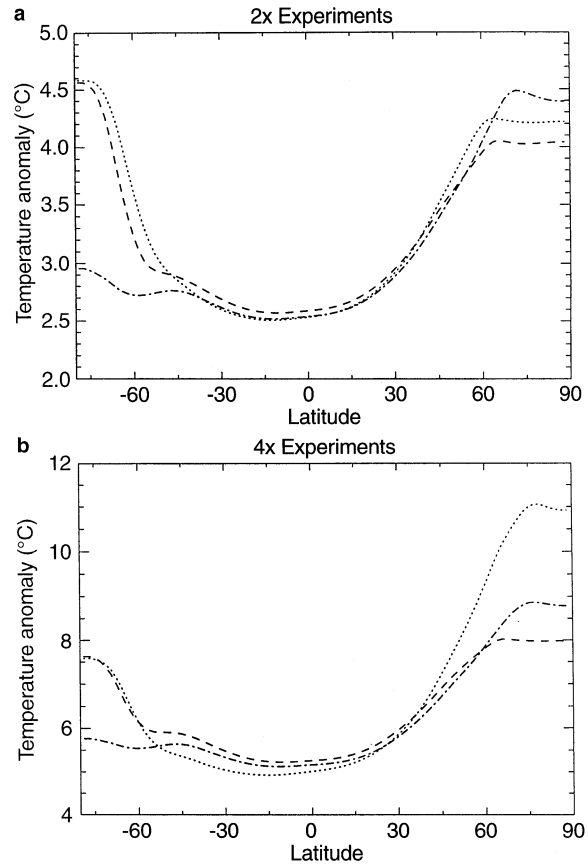

Fig. 9a, b Zonal profiles of the average surface air temperature response for **a** the 2x **a** and **b** 4x experiments. The H, HBL and GM model responses are shown with *dash-dotted*, *dashed* and *dotted lines*, respectively

which allows for the amplification of the $2 \times CO_2$ response. In all cases (H2x, HBL2x, GM2x), the North Atlantic overturning (Fig. 6), and hence northward heat transport (Fig. 10), increased at the $2 \times CO_2$ equilibrium, such that the ocean acted locally in the Northern Hemisphere as a positive feedback to warming.

In the equilibrium $4 \times CO_2$ case (Fig. 8), the ice-albedo feedback continues to be the dominant process leading to interhemispheric symmetry in the HBL4x and GM4x cases, and asymmetry in the H4x case (where there is little ice in the Southern Hemisphere control climatology). The maximum annually-averaged warming in the Northern Hemisphere now occurs in the GM4x case (rather than H4x), due to a substantial decrease in Northern Hemisphere ice (Fig. 8c) associated with dramatically increased equilibrium overturning (Fig. 6i) and hence northward heat transport (Fig. 10f).

McDougall et al. (1996) suggested that one should expect a reduced efficiency in the uptake of heat by the ocean in response to climate warming when GM-type sub-grid scale mixing is used. The inspection of the globally-averaged equilibrium results (Table 4) suggests that the equilibrium climate response is relatively insensitive to the particular sub-grid scale parametrisation used, although warming is actually slightly reduced in the H2x and H4x cases compared to the GM2x and GM4x cases. While at equilibrium the globally-averaged heat flux is zero, over the region south of 50 °S the air-sea heat flux is 2.9 Wm^{-2} larger in H2x than GM2x, while it is 2.1 Wm^{-2} larger in HBL2x than GM2x. This suggests that the inclusion of GM has reduced the heat uptake as expected (relative to H and HBL) in the Southern Ocean, which is compensated for by increased heat uptake at other latitudes so that the global average is zero. Nevertheless, the impact of the ice-albedo feedback in the GM case swamps the local reduction in heat uptake, and so is primarily responsible for the strong warming that occurs there. In the next section we will examine the transient response of this Southern Ocean heat uptake more closely.

5 The transient 2× and 4×CO_2 climate response

In this section we focus our attention on three aspects of the transient response of the climate system to increasing anthropogenic greenhouse gases. We begin by examining the transient response of the North Atlantic thermohaline circulation, focusing on the importance of heat versus freshwater flux forcing. We then

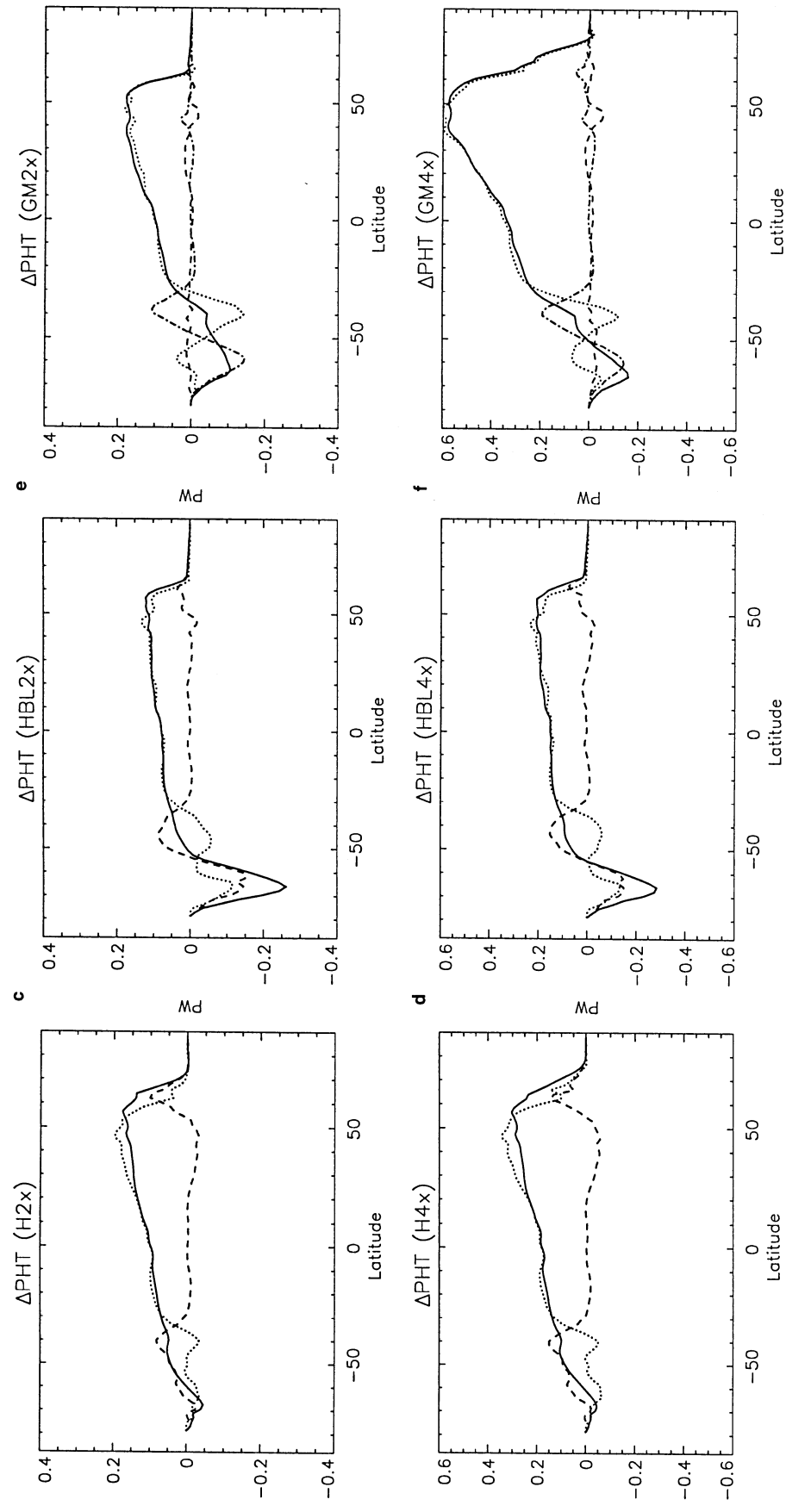

Fig. 10a–f Global ocean poleward heat transport changes relative to the present-day control integration (PW; *positive values* indicate northward transport) for the $2\times$ and $4\times CO_2$ experiments. **a** H2x; **b** H4x; **c** HBL2x; **d** HBL4x; **e** GM2x; **f** GM4x. The advective, diffusive and eddy-induced bolus transport terms are indicated by *dotted*, *dashed* and *dash-dotted lines*, respectively. The total transport is given by the *solid line*

re-address the issue of heat uptake efficiency through an intercomparison of the results from our suite of three models. Finally, we examine the intrusion of subsurface warm water into the Arctic Ocean which we find in our model experiments.

5.1 North Atlantic thermohaline circulation

As noted in the previous section, the equilibrium $2 \times Co_2$ and $4 \times CO_2$ overturning in the North Atlantic was stronger than the climatological overturning in all cases (H, HBL, GM), which, through enhanced ocean heat transport, represents a positive equilibrium feedback to high northern latitude warming. The sign of the ocean feedback is negative in the earlier stages of the transient integration (Fig. 11), where in all cases a reduction in overturning strength ensues once the radiative forcing starts to increase. This reduction during the early part of the transient phase is consistent with the results of most coupled atmosphere-ocean GCMs (IPCC 1995). The reestablishment of thermohaline circulation in all the $4 \times CO_2$ experiments to values higher than their respective present-day climatological values is, however, in contrast with the results of Manabe and Stouffer (1993). In their $4 \times CO_2$ experiment the overturning collapsed completely, although it recovered after about 3000 years.

The transient phase of the $4 \times CO_2$ integration over the first 70 y (by which point a doubling of CO_2 has been reached) is identical to the corresponding $2 \times CO_2$ integrations. The H models (Fig. 11a) show the great reduction in overturning strength, reaching almost 3 Sv (12%) at the time of CO_2 quadrupling. In the HBL4x case (Fig. 11b), the drop is only 1.6 Sv (once more representing a 12% drop relative to the present-day climatology), whereas in the GM case (Fig. 11c) it is only 1.1 Sv (about 8.5%). The GM results are unique in that unlike the H and HBL cases, the reduction does not continue past the point of CO_2 doubling. In GM4x the overturning begins to increase more rapidly than in GM2x shortly after CO_2 doubling is reached. In the H4x and HBL4x cases, the strength of the overturning continues to diminish as the CO_2 concentration increases from $2\times$ to $4 \times CO_2$.

Through the Clausius-Clapeyron equation, a warmer atmosphere implies a higher saturation specific humidity. As such, consistent with coupled GCMs (IPCC 1995), our suite of experiments all reveal an intensification of the hydrological cycle with enhanced net tropical evaporation, poleward moisture transport, and subsequent net middle-high latitude precipitation, especially in the Northern Hemisphere (Figs. 12 and 13). Since the haline forcing (precipitation minus evaporation) acts to *brake* the North Atlantic overturning, and thermal forcing (heat exchange) acts to *drive* it (see e.g. Weaver 1995), the weakening and subsequent reestablishment is largely due to the transition from the dominance of increased high-latitude freshening to increased low-latitude warming. The result of this transition is an increased meridional density contrast which (see next section) causes the weakened North Atlantic overturning to recover and surpass its initial strength. In the case of Manabe and Stouffer (1993) the opposite dominance occurs and the overturning (in the $4 \times CO_2$ scenario) remains weak. Parallel experiments with the wind stress feedback turned on did not greatly effect the weakening/reestablishment time scale or its

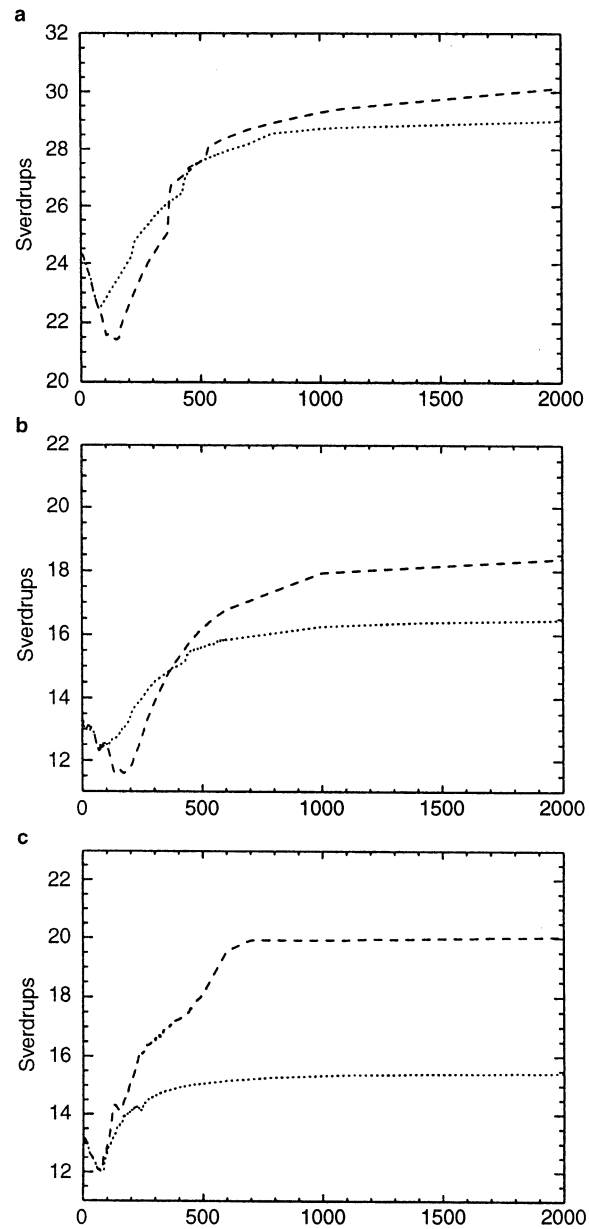

Fig. 11a–c Maximum North Atlantic overturning strength (Sv) as a function of time for the first 2000 y of integration of the **a** H experiments; **b** HBL experiments; **c** GM experiments. The *dotted* and *dashed lines* indicate the $2\times$ and $4\times$ CO_2 experiments, respectively. The time of CO_2 doubling (quadrupling) is 70 (140) y. Note that the mean velocities only are used in the GM case

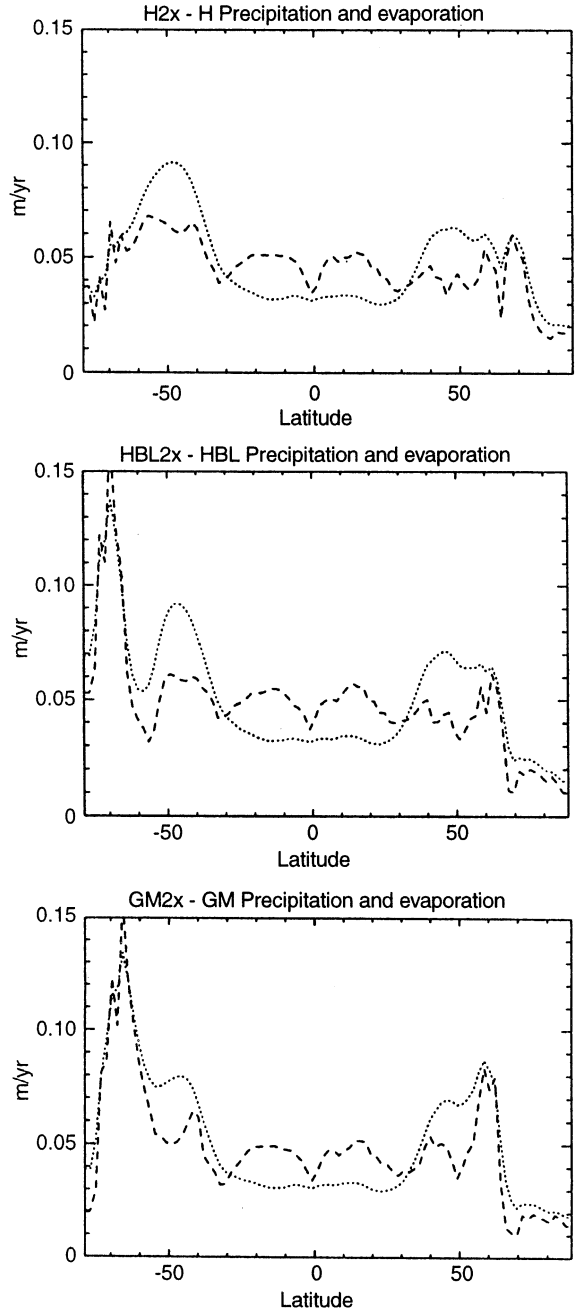

Fig. 12 Anomalous zonal mean evaporation (*dashed line*) and precipitation (*dotted line*) for the three 2x experiments

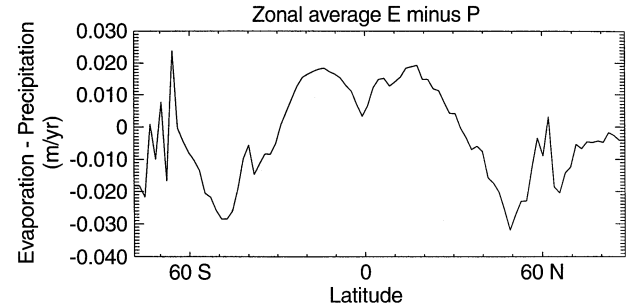

Fig. 13 Difference (relative to the control) of the zonally-averaged evaporation minus precipitation (m/y) at the equilibrium of the GM2x experiment (GM2x-GM). The H2x and HBL2x models are qualitatively similar

magnitude, so that wind-feedbacks through enhanced Ekman and gyre oceanic salt transport are not crucial to our results.

The reduction that we find in the transient phase of all CO_2-increase experiments is less than that found in several coupled atmosphere-ocean GCMs (e.g. Manabe et al. 1991; Manabe and Stouffer 1993; Murphy and Mitchell 1995; Gordon and O'Farrel 1997). This may be partially related to the fact that these coupled models employ flux adjustments to maintain a stable equilibrium present-day climate. That is, if a perturbation caused a slight reduction in the intensity of convection (or a horizontal shifting of its location, Lenderink and Haarsma 1994), then the flux adjustment could act as a positive feedback, applying extra freshwater where it was needed in the control integration. Since there is no effective mechanism for the removal of sea surface salinity (SSS) anomalies, this process would further reduce convection until a balance was reached in the ocean (e.g., through enhanced Ekman and gyre freshwater transport away from the now stratified convective region). Since the flux adjustment issue is not likely to shed light on our response relative to those of coupled atmosphere-ocean GCMs, we turn to the role of changes in surface buoyancy forcing.

As noted earlier, the thermohaline circulation is driven by the competing effects of thermal and freshwater forcing. In response to increasing CO_2, the hydrological cycle intensifies, resulting in increased net precipitation at high latitudes and evaporation in the tropics (Fig. 13). In addition, the SAT response is magnified at high latitudes (largely due to an ice-albedo feedback). Due to the nonlinearity of the equation of state, density of cold water (i.e. at high latitudes) only depends weakly on temperature. As such, small salinity perturbations have a more significant effect than thermal perturbations on density. For warmer temperatures (i.e. at low latitudes), temperature changes affect the density more strongly. The dynamic response of the termohaline circulation is then determined by the changing meridional density gradient resulting from the competing effects of thermal versus freshwater flux forcing.

To investigate this issue more thoroughly, we now examine the evolution of the surface density flux throughout the transient phase of our integrations. Heat and freshwater fluxes were combined to create density fluxes (F_ρ) following Gill (1982) and Schmitt et al. (1989):

$$F_\rho = \frac{\alpha Q}{C_w} + \beta\rho(E - P)S, \tag{2}$$

where Q is the upward heat flux, C_w is the specific heat of water and ρ its density, $E - P$ is the difference between evaporation and precipitation (m/s), S is the salinity in psu and α and β are the thermal and haline expansion coefficients for sea water, given respectively by:

$$\alpha = -\frac{1}{\rho}\frac{\partial \rho}{\partial T}, \qquad \beta = \frac{1}{\rho}\frac{\partial \rho}{\partial S}. \tag{3}$$

Equations 2 and 3 give the density flux in units of mass per unit area per unit time, with $F_\rho > 0$ implying that the surface layer is gaining mass. Using annual mean, zonally-averaged SST, SSS, Q, and $E - P$ in the Atlantic Ocean, we calculated α and β, and hence F_ρ, every five years for the first 300 y of integration of the 2x experiments (H2x, HBL2x, GM2x). Since the results for H2x and HBL2x were qualitatively similar, we focus our attention on GM2x (Fig. 14).

During the early phases of the transient integration, changes in the hydrological cycle caused increased high latitude North Atlantic freshening (Fig. 14b) at the expense of low-latitude evaporation (Fig. 14d). This freshening reduces high-latitude convection and hence the meridional overturning (Fig. 11c). Initially the ocean acts as a negative feedback in the high-latitude North Atlantic, counteracting the radiative forcing associated with the increasing levels of atmospheric CO_2. At lower latitudes the effects of increasing atmospheric CO_2 add buoyancy to the surface of the ocean (Fig. 14c–d), until the forcing is held fixed (around 70 y) and the climate system is allowed to approach equilibrium. The reestablishing North Atlantic overturning transports anomalously (relative to the control climate) warm waters poleward so that the ice edge starts to melt back. As such, the sea surface, once insulated from the atmosphere by sea ice, is now able to release heat and so the density flux is increased, eventually dominating over the high-latitude freshening to create a negative buoyancy flux (Fig. 14b). The increasingly positive density flux at high latitudes acting in concert with the increasingly negative density flux at low latitudes, acts to further increase the overturning to values greater than the respective present-day climatologies. The North Atlantic ocean now acts as a positive feedback to enhance local warming.

In order to help separate the high- and low-latitude effects we now examine the depth-integrated steric

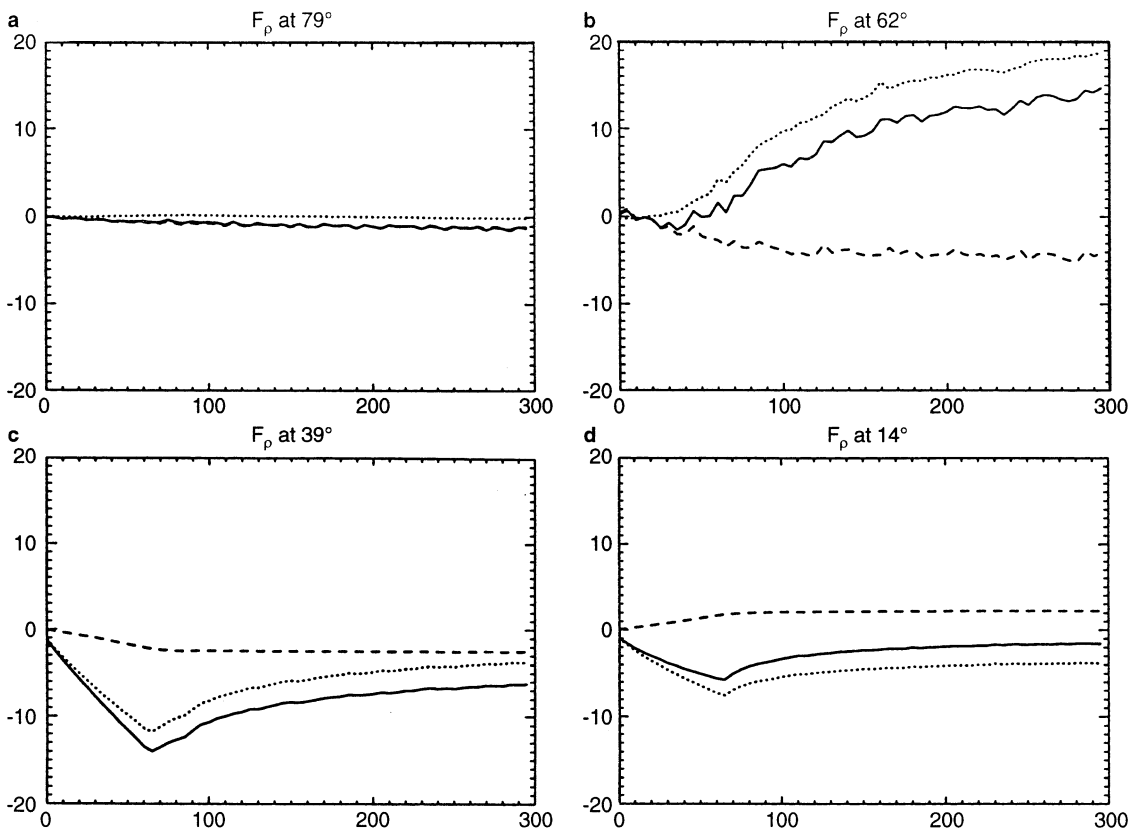

Fig. 14a–d Surface density fluxes (10^{-8} kgm^{-2}s^{-1}) in four latitude bands in the North Atlantic during the transient of the GM2x experiment. The horizontal axis gives the time in years from the beginning of the $2 \times CO_2$ experiment. **a** covers the arctic (70 °N–90 °N); **b** covers the deep water formation region (50 °N–70 °N); **c** covers the mid-latitudes (25 °N–50 °N); **d** covers the tropics (0 °N–25 °N). The *solid line* is the density flux which is decomposed into its haline component (*dashed*) and thermal component (*dotted*)

Table 5 Equilibrium zonally-averaged depth-integrated steric height (Φ) and corresponding changes in the North Atlantic overturning strength (Ψ) in the three families of models. The model experiment is listed in column 1. Columns 2 and 3 give the depth integrated steric height (relative to 925 m and scaled by ρ_0) at the latitude of maximum zonally-averaged surface density and the Equator, respectively. The difference between columns 2 and 3 is given in column 4. Column 5 gives the maximum value of North Atlantic overturning and column 6 gives the increase relative to the respective control experiment. Columns 7 and 8 show the percentage increase of the depth integrated steric height gradient and overturning strength compared to the control climatology of each suite. The final column shows the ratio of column 4 to column 5 confirming the near linear dependence of overturning rate to meridional depth-integrated steric height gradient

Model	Φ_S (10^{-6} kgm^{-1})	Φ_N (10^{-6} kgm^{-1})	$\Delta_{S-N}\Phi$ (10^{-6} kgm^{-1})	Ψ Sv	$\Delta\Psi$ Sv	% increase $\Delta_{S-N}\Phi$	% increase $\Delta\Psi$	$\Delta_{S-N}\Phi/\Psi$
H	1.72	1.48	0.24	24.3				0.010
H2x	1.80	1.45	0.36	29.2	4.9	49	20	0.012
H4x	1.90	1.45	0.45	30.9	6.6	86	27	0.015
HBL	1.65	1.47	0.18	13.1				0.014
HBL2x	1.72	1.51	0.21	16.6	3.5	18	27	0.013
HBL4x	1.80	1.56	0.25	18.6	5.5	37	42	0.013
GM	1.69	1.47	0.22	13.2				0.017
GM2x	1.80	1.51	0.29	15.4	2.3	29	17	0.019
GM4x	1.90	1.55	0.35	20.0	6.9	56	52	0.018

height Φ, defined by:

$$\Phi = \int_{z_0}^{0} \int_{z_0}^{z'} \left(\frac{\rho_0 - \rho(T,S,P)}{\rho_0} \right) \mathrm{d}z' \, \mathrm{d}z, \tag{4}$$

where ρ_0 is a reference density and $\rho(T, S, P)$ is the *in situ* potential density. The depth integrated steric height (Φ) gives a measure of the depth-integrated pressure above a reference level (scaled by g^{-1}, the inverse of the acceleration due to gravity), yielding a cumulative measure of the ocean response to the density fluxes discussed already. When the net density flux over time is positive into the surface of the ocean, Φ will decrease. Hughes and Weaver (1994) showed that for a suite of ocean GCM configurations the maximum strength of the overturning in the Atlantic Ocean was approximately linearly proportional to the meridional difference in zonally-averaged Φ. Table 5 illustrates this result for all of our equilibrium climatologies, although here the difference is taken between the latitude of maximum zonally-averaged surface density in the north and the Equator. The GM and HBL model experiments verify the linear dependence although the H suit of experiments are less linear. This is likely due to breakdown in our assumption of the existence of a constant level of no motion (925 m) in the H case (with the most vigorous overturning).

The annual mean, zonally-averaged, depth-integrated steric height field (relative to 925 m) clearly summarises the equilibrium Atlantic Ocean response to the competing effects of heat and freshwater flux forcing (shown for GM in Fig. 15). In the South and tropical Atlantic, there is a near linear increase in depth-integrated steric height (relative to the control climatology) with increasing equilibrium atmospheric CO_2 levels. Changes at the high northern latitudes, while also linear with increasing CO_2, are much smaller than at lower latitudes (due to enhanced high-latitude precipitation and the dominance of salinity changes over temperature changes at low temperatures in the equation of state). In response to the increased meridional depth-integrated steric height gradient, the overturning in the North Atlantic also increased relative to the present-day control climatology.

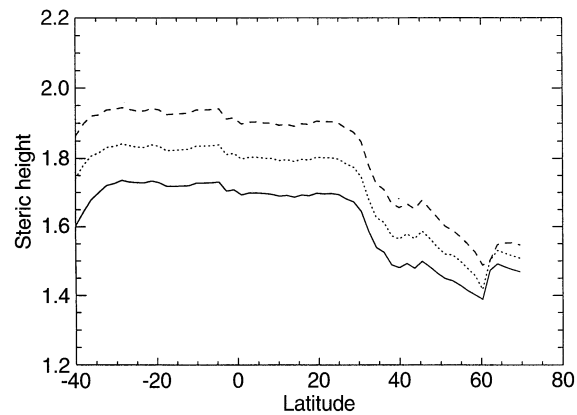

Fig. 15 Zonally-averaged annual mean Atlantic depth-integrated steric height (relative to 925 m; 10^{-6} kgm^{-1}) at the equilibrium climatologies of GM (*solid line*), GM2x (*dotted line*) and GM4x (*dashed line*)

5.2 Efficiency of heat uptake

McDougall et al. (1996) found that the global efficiency of the uptake of a passive tracer was 77% larger (after 20 y) in an H-type case relative to a GM-type case. Most of this increase arose from changes in the Southern Ocean where the efficiency was 100% larger. They further suggested that this factor should carry over into

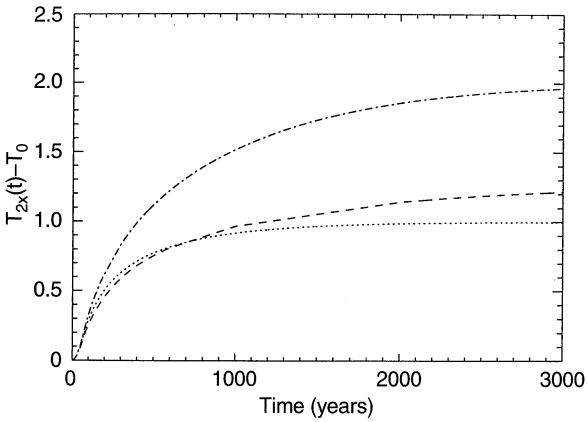

Fig. 16 Difference between the volume-averaged global ocean potential temperature from the transient $2 \times CO_2$ runs and the respective control runs. The H2x-H, HBL2x-HBL and GM2x-GM cases are given by the *dashed-dotted*, *dashed* and *dotted lines*, respectively

the SAT response of a coupled model in response to increasing atmospheric CO_2, provided that the air-sea heat flux was similar both with and without the additional eddy parametrisation. We now look at this issue more carefully through an examination of the transient oceanic heat uptake in our suite of experiments (H, HGL, GM).

The volume-averaged global ocean potential temperature change (relative to the control experiments) as a function of time through the transient CO_2-increase experiments (Fig. 16), confirms the result that the Gent and McWilliams (1990) parametrisation reduces the efficiency of heat uptake relative the the H2x case. In fact this is the case throughout the transient phase of the GM2x experiment, where globablly-averaged equilibrium ocean temperatures warmed about half as much as in H2x. Interestingly, the reduced efficiency of the GM2x case is also associated with a faster equilibration time-scale to the imposed radiative forcing perturbation. The reduced near-surface vertical diffusivity in HBL2x is, on the other hand, the most effective of all in reducing globally-averaged heat uptake efficiency during the first 700 y of the transient integration. Eventually the ocean in HBL2x is also warmer than in GM2x, although the equilibration time-scale is much longer. GM2x shows the smallest change of the three experiments as it is the most effective in isolating surface changes from the deep ocean. When lateral mixing is used (H and HBL), spurious convection can arise when heat is diffused poleward across outcropping isopycnals (i.e. at high latitudes). In GM, mixing is aligned along isopycnals so convection is substantially reduced.

The decreased global heat uptake efficiency is in agreement with the ocean-only GCM results of McDougall et al. (1996), as well as the coupled model results of Hirst et al. (1996). The magnitude of this decreased efficiency is, however, substantially smaller in our case than in McDougall et al. (1996), and is more in line with the findings of Hirst et al. (1996). After 20 y, there is only a 5% difference is globally-averaged ocean temperature change between GM2x and H2x. The use of restoring boundary conditions (and implied infinite heat capacity atmosphere) in McDougall et al. (1996) probably overestimates differences in the uptake of passive traces in convective regions (where the restoring boundary conditions create large heat fluxes).

5.3 Intrusion of warm water into the arctic

An intriguing result found in our increasing atmospheric CO_2 experiments, under GM and HBL subgrid scale mixing, was the subsurface intrusion of warm North Atlantic waters into the arctic (Fig. 17). After 300 years in the HBL2x experiment the entire arctic at 900 m is warmed by more than 0.25 °C. Water warmed by more than 0.75 °C has also reached the North Pole. In the GM2x case, the warm water intrusion is less extensive, with water warmed by about 0.25 °C reaching the North Pole by 300 y. While the H2x model has distinct surface warming, there is no apparent subsurface warm water intrusion north of 75°.

The mechanism for warming in both the HBL2x and GM2x experiments is quite similar and initially involves enhanced subsurface transport of warm Atlantic waters into the arctic. The arctic is not well represented in our coupled model so that the Atlantic waters enter an environment of relatively weak circulation where further spreading occurs on slow advective and diffusive time scales. In the H2x case, there is enhanced intrusion of the surface waters (Fig. 6a–c) which dramatically melts back the ice edge (Fig. 7a), exposing the ocean surface to the cold polar air. Strong convection then wipes out the signature of the warm Atlantic waters entering the arctic. The ice edge in the HBL2x and GM2x cases is not as greatly affected in the $2 \times CO_2$ equilibrium climates (Figs. 7b–c).

The initial enhancement of subsurface transport of Atlantic waters into the arctic (across 70 °N) in the H2x, HBL2x and GM2x experiments is portrayed in Fig. 18. As there is only one oceanic connection between the arctic and the rest of the world oceans, transport across this latitude sums to zero over depth. In all three cases there is enhanced surface intrusion by 50 y with return flow at deeper levels. In the HBL2x case, a subsurface local maximum near 1400 m develops and intensifies slightly with time (Fig. 18e, f). A similar subsurface maximum of northward transport develops in the GM2x case (Fig. 18h, i), although at slightly shallower depth. In both the GM2x and HBL2x experiments, the subsurface ocean remains insulated from the polar air (due to the existence of sea ice at the surface) throughout the transient CO_2 integration, which is not the case in the H2x experiment. During the initial stages (first 50 y) H2x and HBL2x have very similar transport

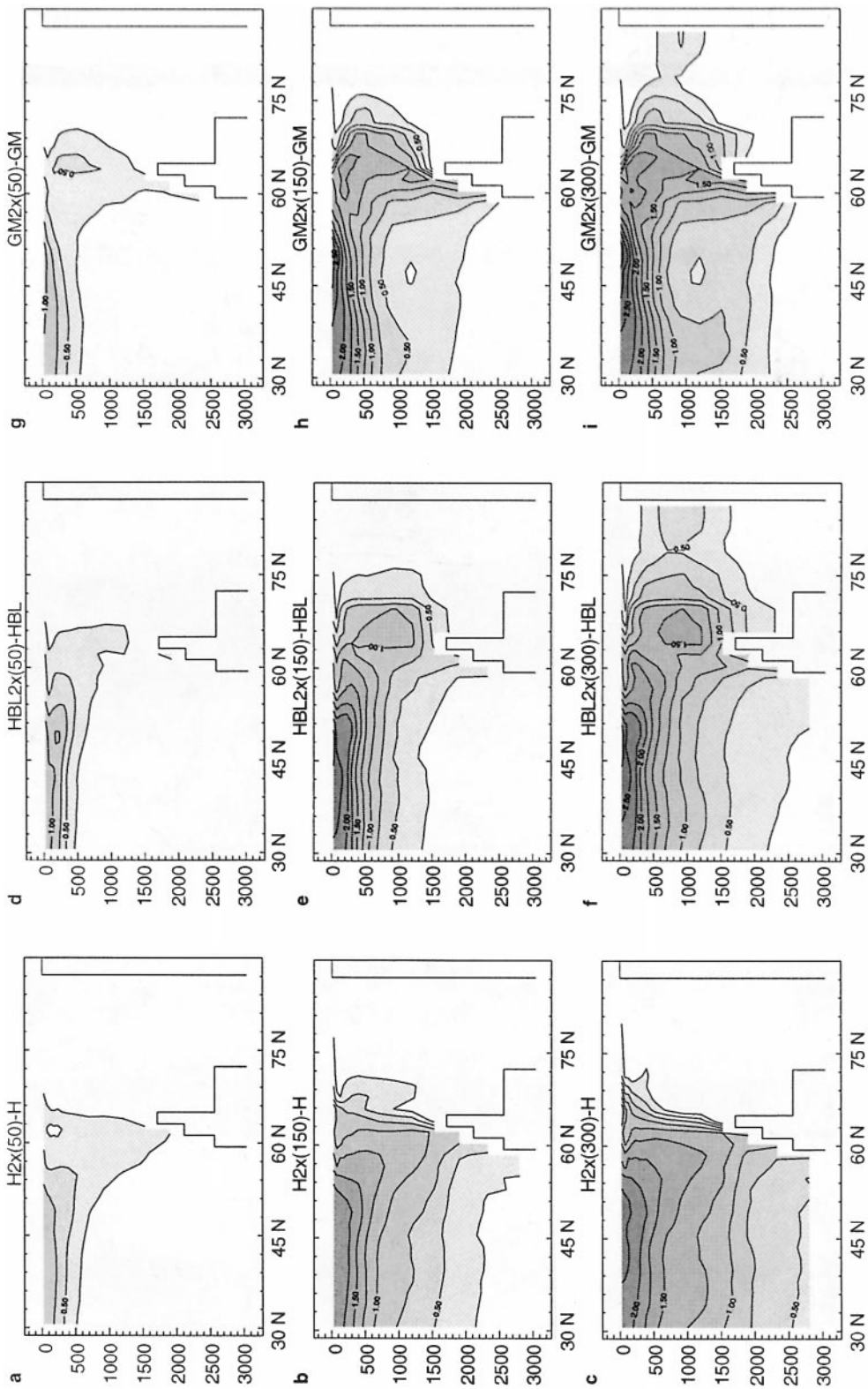

Fig. 17a–i Zonally-averaged ocean potential temperature for three 2x experiments at high northern latitudes (contour interval is 0.25 °C). **a–c** H2x at 50 y, 150 y and 300 y respectively; **d–f** as in **a–c** but for HBL2x; **g–i** as in **a–c** but for GM2x

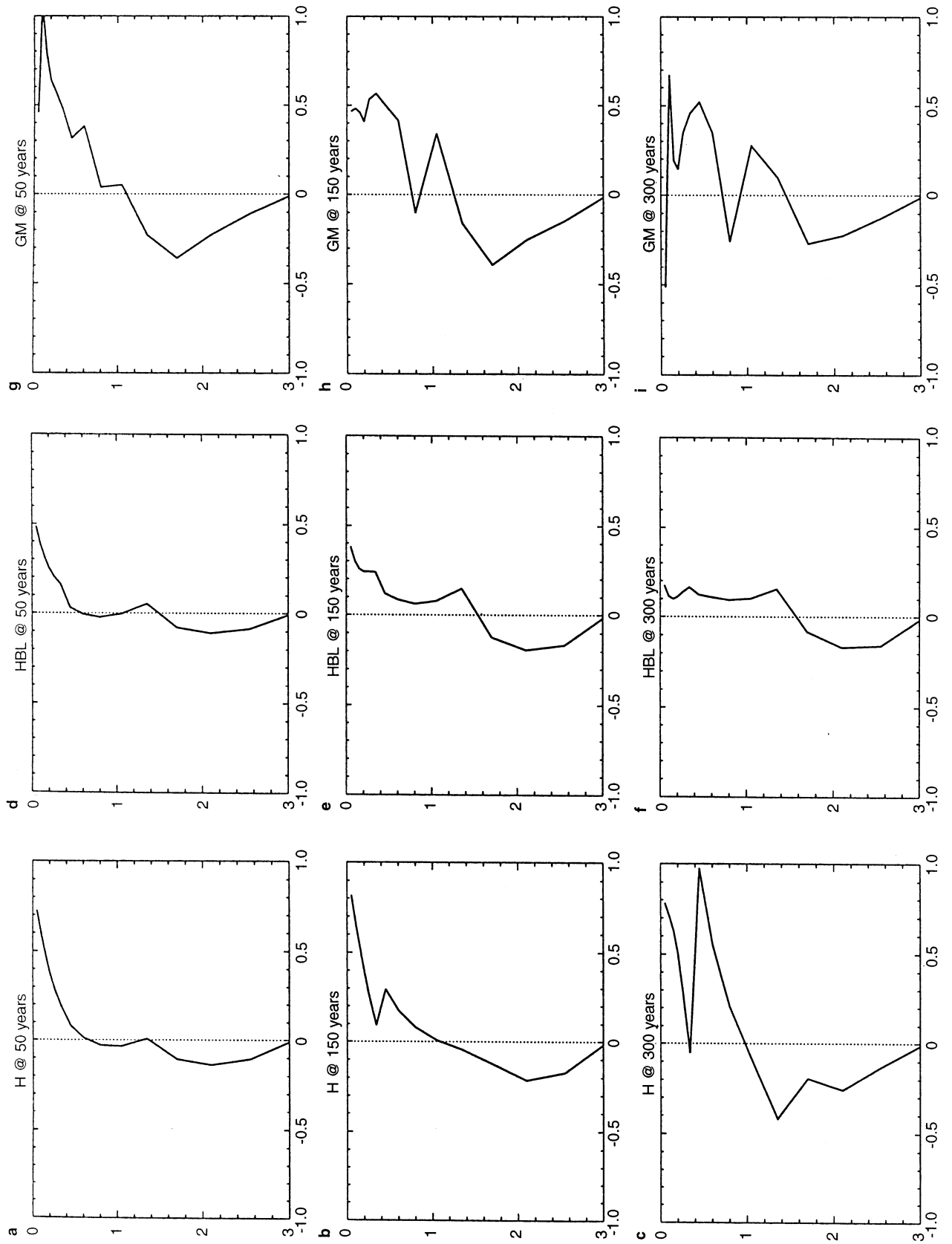

Fig. 18a–i Annual mean difference between the $2 \times CO_2$ and control model transport across 70 °N in the North Atlantic. The horizontal axis gives transport in cm/s with *positive values* indicating northward transport, while the vertical axis corresponds to depth in km. **a–c** H2x-H at 50 y, 150 y and 300 y, respectively. **d–f** as in **a–c** but for HBL2x-HBL; **g–i** as in **a–c** but the GM2x-GM

profiles (Fig. 18a, d), with a local subsurface maximum developing in H2x as well. The strong northward transport in the near surface regions of the H2x experiment, however, melts back the sea ice, thereby exposing the ocean surface to cold polar air which initiates vigorous convection, mixing the water column vertically.

Once the warm waters enter the arctic they spread both advectively and diffusively. Using an advective velocity scale of $U = 0.1\ \mathrm{cm\,s^{-1}}$ (Fig. 18f) as representative of the subsurface transport, and an along-path length scale $L = 2.2 \times 10^6$ m (20° of latitude), gives an advective time-scale of $T_a \sim \frac{L}{U} = 70$ y. The time-scale for diffusive spreading of the warmed waters, once they are present in the arctic, is $T_d \sim \frac{L^2}{k_h}$, where k_h is the horizontal (or isopycnal in GM) diffusivity. Setting $k_h = 2 \times 10^3\ \mathrm{m^2\,s^{-1}}$ gives $T_d \sim 80$ y, which is similar to T_a. Both these time-scales are consistent with the intrusion time-scale seen in the HBL2x model, although they are somewhat too fast for the GM2x model. This is possibly due to the fact that isopycnal surfaces are not aligned horizontally in the arctic so that the isopycnal diffusion (GM) differs substantially from horizontal diffusion (HBL). As such, the *effective* k_h in GM2x is substantially smaller than $k_h = 2 \times 10^3\ \mathrm{m^2\,s^{-1}}$. The subsurface transport in GM2x is, however, stronger than in the HBL2x case, so that the advectice time-scale is shorter. Vertical diffusion, whose effects would be to slowly remove thermal anomalies, is larger in GM2x than in HBL2x and so may also be responsible for the diminished signal in GM2x.

6 Summary

We have explored the sensitivity of global warming experiments to the parametrisation of sub-grid scale ocean mixing. This was accomplished using an EMBM coupled to a thermodynamic sea ice model and an OGCM, in which three distinct sub-grid scale tracer mixing schemes were used: (1) Laplacian diffusion with constant horizontal and vertical diffusivities (H); (2) Laplacian diffusion with a constant horizontal diffusivity and a vertically-varying vertical diffusivity taken from Bryan and Lewis (1979) (HBL); (3) the Gent and McWilliams 1990 scheme (GM). The computational efficiency of our coupled model allowed us to integrate the coupled system through the transient phase of CO_2-increase until a new equilibrium was reached.

The climate sensitivity of all three classes of models was a 3.0 °C increase in globally-averaged, annual mean SAT for a doubling of atmospheric CO_2, within the range of estimates provided by IPCC (1995). The similarity of the global mean equilibrium $2 \times CO_2$ and $4 \times CO_2$ SST and SAT, in models using three distinct sub-grid scale mixing schemes, suggests that at equilibrium, the ocean provides little global climate feedback. This is of course not true on the regional scale or during the transient phase of the integrations where significant differences exist between model classes.

In the initial stages of the transient phase of all of our CO_2 experiments the thermohaline circulation in the North Atlantic reduces, due to an enhancement of the hydrological cycle and subsequent increase in mid-high-latitude precipitation. The weakened overturning, however, reestablishes in all cases to surpass its climatological strength. This occurs due to the eventual dominance of low-latitude warming over high-latitude freshening leading to an increased meridional depth-integrated steric height gradient. A secondary positive feedback also occurs during the reestablishment process. As the conveyor builds in strength its northward transport of heat also increases, which, together with high-latitude CO_2-induced radiative warming, melts back the sea-ice edge. The newly exposed ocean water is no longer insulated from the atmosphere and so loses buoyancy, thereby reinforcing the strengthening conveyor. This process continues until a new equilibrium, with stronger overturning, is reached. At equilibrium the ocean therefore provides a positive feedback to regional North Atlantic warming, through enhanced heat transport, in both the $2 \times CO_2$ and $4 \times CO_2$ cases. During the early phases of the transient response, the sign of the ocean feedback is negative through reduced ocean heat transport associated with a weakening conveyor.

We also examined whether or not the incorporation of the Gent and McWilliams (1990) parametrisation reduced the efficiency of oceanic heat uptake during the transient phase of CO_2-increase experiments, as implied by McDougall et al. (1996). In accordance with expectations, the H experiments were more effective in taking up heat compared to the GM case, although not as effective as in the uncoupled ocean-only experiments of McDougall et al. (1996). Unlike Hirst et al. (1996), however, we found a symmetric climate response to increasing atmospheric CO_2 in the GM (and HBL) experiments. This symmetric response in GM and HBL, and asymmetric response in H, was largely due to the existence of more realistic sea ice in the climatological control integrations and the subsequent enhanced ice-albedo feedback upon warming.

In our transient CO_2-increase experiments using the GM and HBL mixing schemes, subsurface warm waters were found to intrude into the arctic. This arctic intrusion was not found in the H2x case due to the onset of enhanced high-latitude North Atlantic convection, which rapidly mixed the water column as the ice edge retreated. Once in the arctic, these waters were slowly advected and diffused throughout the basin, filling the middle layers with an anomalously warm water mass of Atlantic origin. This warming of the mid-depth Arctic Ocean is qualitatively similar to recent observed patterns of subsurface Arctic Ocean warming (Carmack et al. 1995). While the magnitude of anomalous warming in our model is similar to these

observations, the intrusion time-scale and depth of maximum warming is not. The lack of a proper representation of the Arctic Ocean in our model severely limits our ability to quantitatively capture the dynamics of the region. Nevertheless, it is interesting that the observed warming trend is consistent with our model response to increasing atmospheric CO_2.

In summary, we have attemped to emphasise the importance of the parametrisation of sub-grid scale mixing on the transient evolution and regional response of the climate system to increasing anthropogenic greenhouse gases. While apparently of little importance to the climate sensitivity of the global coupled system, small-scale processes in the ocean can feed back on the basin-scale ocean circulation to cause substantial differences in model solution depending on how they are parametrised. As such, increased understanding of the basic physics and parametrisation of these unresolved ocean processes is important in order to improve the realism of regional climate change forecasts from coupled GCMs.

Acknowledgements This research was supported by NSERC Strategic, Steacie and Operating grants as well as funding through the Canadian Institute of Climate Studies and an IBM SUR grant. All computations were conducted on a suite of IBM RS6000s including two IBM SPs. Infrastructure support from the University of Victoria is also gratefully acknowledged. The authors are grateful to M. Eby, A. Fanning and G. Flato for discussions and advice concerning this work.

References

Böning CW, Holland WR, Bryan FO, Danabasoglu G, McWilliams JC (1995) An overlooked problem in model simulations of the thermohaline circulation and heat transport in the Atlantic Ocean. J Clim 8:515–523

Bryan F (1987) Parameter sensitivity of primitive equation ocean general circulation models. J Phys Oceanogr 17:970–985

Bryan K, Lewis LJ (1979) A water mass model of the World Ocean. J Geopohys Res 84:2503–2517

Carmack EC, MacDonald RW, Perkin RG, McLaughlin FA, Pearson RJ (1995) Evidence for warming of Atlantic water in the southern Canadian Basin of the Arctic Ocean: results from the Larsen-93 expedition. Geophys Res Lett 22:1061–1064

Danabasoglu G, McWilliams J (1995) Sensitivity of the global ocean circulation to parametrization of mesoscale tracer transports. J Clim 8:2967–2987

Danabasoglu G, McWilliams JC, Gent PR (1994) The role of mesoscale tracer transports in the global ocean circulation. Science 264:1123–1126

da Silva AM, Young CC, Levitus S (1994) Atlas of marine data 1994. Vol 3: anomalies of heat and momentum fluxes. NOAA Atlas NESDIS 8, US Department of Commerce, NOAA, NESDIS, Washington, DC, pp 99

England MH (1995) Using chlorofluorocarbons to assess ocean climate models. Geophys Res Lett 22:3051–3054

Fanning AF, Weaver AJ (1996) An atmospheric energy-moisture balance model: climatology, interpentadal climate change, and coupling to an ocean general circulation model. J Geophys Res 101:15111–15128

Fanning AF, Weaver AJ (1997a) Temporal-geographical meltwater influences on the North Atlantic conveyor: implications for the Younger Dryas. Paleoceanogr 12:307–320

Fanning AF, Weaver AJ (1997b) On the role of flux adjustments in an idealized coupled climate model. Clim Dyn 13:691–701

Fanning AF, Weaver AJ (1997c) A horizontal resolution and parameter sensitivity study of heat transport in an idealized coupled climate model. J Clim 10:2469–2478

Gent PR, McWilliams J (1990) Isopycnal mixing in ocean circulation models. J Phys Oceanogr 20:150–155

Gill A (1982) Atmosphere-ocean dynamics. Academic Press, London, pp 662

Gordon HB, O'Farrel SP (1997) Transient climate change in the CSIRO coupled model with dynamic sea ice. Mon Weather Rev 125:875–907

Graves CE, Lee WH, North GR (1993) New parametrizations sensitivities for simple climate models. J Geophys Res 98:5025–5036

Griffes AM, Gnanadesikan A, Pacanowski RC, Larichev VD, Dukowicz JK, Smith RD (1998) Isoneutral diffusion in a z-coordinate model. J Phys Oceanogr 28:805–830

Hartman DL (1994) Global physical climatology. Academic Press, San Diego, pp 411

Hibler WD III (1979) A dynamic thermodynamic sea ice model. J Phys Oceanogr 9:815–846

Hirst AC, Gordon HB, O'Farrel SP (1996) Global warming in a coupled climate model including oceanic eddy-induced advection. Geophys Res Lett 23:3361–3364

Hughes TMC, Weaver AJ (1994) Multiple equilibria of an asymmetric two-basin ocean model. J Phys Oceanogr 24:619–637

Intergovernmental Panel on Climate Change (1990) Climate change: the IPCC scientific assessment. Cambridge University Press, Cambridge, UK, pp 366

Intergovernmental Panel on Climate Change (1992) Climate change 1992, the supplementary report to the IPCC scientific assessment. Cambridge University Press, Cambridge, pp 200

Intergovernmental Panel on Climate Change (1995) Climate change 1995, the science of climate change. Cambridge University Press Cambridge, pp 572

Lenderink G, Haarsma RJ (1994) Variability and multiple equilibria of the thermohaline circulation associated with deep water formation. J Phys Oceanogr 24:1480–1493

Manabe S, Bryan K (1985) CO_2-induced change in a coupled ocean-atmosphere model and its paleoclimatic implications. J Geophys Res 90:11689–11707

Manabe S, Stouffer RJ (1993) Century-scale effects of increased atmospheric CO_2 on the ocean-atmosphere system. Nature 364:215–218

Manabe S, Stouffer RJ (1994) Multiple-Century response of a coupled ocean-atmosphere model to an increase of atmospheric carbon dioxide. J Clim 7:5–23

Manabe S, Stouffer RJ, Spelman MJ, Bryan K (1991) Transient response of a coupled ocean-atmosphere model to gradual changes of atmospheric CO_2. Part 1: annual mean response. J Clim 4:785–818

McDougall TJ, Hirst AC, England MH, McIntosh PC (1996) Implications of a new eddy parameterization for ocean models. Geophys Res Lett 23:2085–2088

Murphy JM, Mitchell JFB (1995) Transient response of the Hadley Centre coupled ocean-atmosphere model to increasing carbon dioxide. Part II: spatial and temporal structure of response. J Climate 8:57–80

Pacanowski R (1995) MOM 2 Documentation, user's guide and reference manual. GFDL Ocean Group Tech Rep 3, GFDL, Princeton, NJ, pp 232

Ramanathan V, Callis L, Cess R, Hansen J, Isaksen I, Kuhn W, Lacis A, Luther F, Mahlman J, Reck R, Schlesinger M (1987) Climate-chemical interactions and effects of changing atmospheric trace gases. Rev Geophys 25:1441–1482

Robitaille DY, Weaver AJ (1995) Validation of sub-grid mixing schemes using CFCs in a global ocean model. Geophys Res Let 22:2917–2920

Russell GL, Millar JR, Rind D (1995) A coupled atmsophere-ocean model for transient climate change studies. Atmos-Ocean 33: 6583–730

Schmitt RW, Bogden PS, Dorman CE (1989) Evaporation minus precipitation and density fluxes for the North Atlantic. J Phys Oceanogr 19: 1208–1221

Semtner AJ (1976) A model for the thermodynamic growth of sea ice in numerical investigations of climate. J Phys Oceanogr 6: 379–389

Thompson SG, Warren SG (1982) Parametrization of outgoing infrared radiation derived from detailed radiative calculations. J Atmos Sci 39: 3667–2680

Weaver AJ (1993) The ocean and global warming. Nature 364: 192–193

Weaver AJ (1995) Driving the ocean conveyor. Nature 378: 135–136

Weaver AJ, Hughes TMC (1996) On the incompatibility of ocean and atmosphere models and the need for flux adjustments. Clim Dyn 12: 141–170

Weaver AJ, Fanning AF, Eby M, Wiebe EC (1998) The climate of the last glacial maximum in a coupled ocean GCM/ Energy-moisture balance atmosphere model, Nature 394: 847–853